PHYSICAL REVIEW D **88,** 054012 (2013)

$K^*\Sigma$ photoproduction off the proton target with baryon resonances

Sang-Ho Kim,[1,2,*] Seung-il Nam,[3,4,†] Atsushi Hosaka,[1,‡] and Hyun-Chul Kim[2,3,§]

[1]*Research Center for Nuclear Physics (RCNP), Osaka 567-0047, Japan*
[2]*Department of Physics, Inha University, Incheon 402-751, Republic of Korea*
[3]*School of Physics, Korea Institute for Advanced Study (KIAS), Seoul 130-722, Republic of Korea*
[4]*Department of Physics, Pukyong National University (PKNU), Busan 608-737, Republic of Korea*

(Received 27 November 2012; published 9 September 2013)

We investigate the photoproduction of $K^{*0}\Sigma^+$ and $K^{*+}\Sigma^0$ off the proton target, employing the effective Lagrangian approach at the tree-level Born approximation. In addition to the (s, t, u)-channel Born diagrams, we take into account various baryon-resonance contributions such as $D_{13}(2080)$, $S_{11}(2090)$, $G_{17}(2190)$, $D_{15}(2200)$, $S_{31}(2150)$, $G_{37}(2200)$, $F_{37}(2390)$, and $\Sigma^*(1385, 3/2^+)$ in a fully covariant manner. We present the numerical results for the energy and angular dependences for the cross sections in comparison to available experimental data. The single-polarization observables, i.e., the photon-beam (Σ_γ), recoil (P_y), and target (T_y) baryon polarization asymmetries are computed as well for future experiments. We observe from the numerical results that the resonance contributions play a minor role in producing the strength of the cross sections, being different from the $K^*\Lambda$ photoproduction. In contrast, it turns out that the $\Delta(1232)$-pole contribution and K exchange in the t channel dominate the scattering process. On the other hand, the higher resonances influence the polarization observables such as the recoil and target asymmetries.

DOI: 10.1103/PhysRevD.88.054012 PACS numbers: 13.60.Rj, 13.60.Le, 13.60.−r, 11.10.Ef

I. INTRODUCTION

Strangeness production via various scattering processes has been one of the most important issues in hadronic and nuclear physics for decades. From them, we can understand the microscopic mechanism of the productions beyond the light-flavor sectors and extend our knowledge into multistrangeness states. In this sense, photoproduction of strange hadrons off the nucleon target is a very useful tool and has been widely studied experimentally as well as theoretically. For example, experiments for the photoproduction of $\gamma N \to K\Lambda$ and $K\Sigma$ were reported in Refs. [1–3]. Related theoretical studies were also performed in Refs. [4–7]. In particular, Ref. [4] emphasized the baryon-resonance contributions, which play important roles in reproducing the experimental data. The effects of the electromagnetic form factor [5] were also investigated for the photo- and electroproduction of the kaon, the Ward-Takahashi (WT) identity being explained. It was also pointed out that the tensor-meson exchange in the t channel provides a significant contribution to kaon photoproduction [6]. An unbiased model selection, based on Bayesian inference, was introduced for extracting physical information from kaon photoproduction [7]. References [8,9] examined the t-channel Regge trajectories to enhance the model's applicabilities to actual problems.

Photoproduction of the vector strange meson (K^*) provides even richer physics in comparison with the KY channel. For instance, since it is a vector meson with quantum number $I(J^P) = 1/2(1^-)$, the exchange of the strange scalar meson κ is allowed in the t channel, which is absent in the KY channel, in addition to (K, K^*) exchanges. Moreover, the polarization of the K^* meson in the final state can be taken as an important subject to be investigated together with other polarization observables in terms of the spin-density matrices. Experimentally, this production channel has been investigated for $\gamma N \to K^*\Lambda(1116)$ by the CLAS Collaboration at the Thomas Jefferson National Accelerator Facility (Jefferson Lab) [10,11], and $\gamma N \to K^*\Sigma(1193)$ by the CBELSA/TAPS Collaboration at the Electron Stretcher and Accelerator (ELSA) [12], by the CLAS Collaboration [13,14], and by the LEPS Collaboration at Super Photon Ring-8 GeV (SPring-8) [15]. These two processes have been extensively studied theoretically within the effective Lagrangian approaches [16–19], as well as in the chiral quark model [20]. As mentioned above, it was argued that the κ-exchange should play an important role in the production mechanism of $\gamma p \to K^*\Sigma$ [17]. Interestingly enough, the recent LEPS experiment reported the experimental data that supported the importance of the scalar-meson exchange indeed [15]. Moreover, employing the same theoretical framework, Ref. [19] showed that there were some contributions from nucleon resonances to reproduce the experimental data of $\gamma p \to K^{*+}\Lambda$.

Considering all these successful and meaningful theoretical results accumulated so far within the effective Lagrangian method with the resonance contributions taken into account, we want to explore carefully the reaction processes $\gamma p \to K^{*0}\Sigma^+$ and $\gamma p \to K^{*+}\Sigma^0$ in the present

*shkim@rcnp.osaka-u.ac.jp
†sinam@kias.re.kr, sinam@pknu.ac.kr
‡hosaka@rcnp.osaka-u.ac.jp
§hchkim@inha.ac.kr

work. Although the $K^*\Sigma$ photoproduction was already studied theoretically within a similar framework in Ref. [17], we will include various baryon-resonance contributions which were proven to be essential in the $K^*\Lambda$ channel [19]. Thus, we introduce the baryon resonances as follows: $D_{13}(2080)$, $S_{11}(2090)$, $G_{17}(2190)$, $D_{15}(2200)$, $S_{31}(2150)$, $G_{37}(2200)$, and $F_{37}(2390)$ in the s channel and $\Sigma^*(1385)$ in the u channel, in addition to the s channel with $N(940)$- and $\Delta(1232)$-pole contributions; the t channel with κ-, K-, and K^*-exchange contributions; and the u channel with $\Lambda(1116)$- and $\Sigma(1193)$-pole contributions. These resonance contributions have not been taken into account in the previous theoretical work [17] and will be treated in a fully relativistic manner in the present work, as done for the $\gamma p \to K^{*+}\Lambda$ [19].

The coupling strengths for strong and electromagnetic (EM) vertices are computed by using experimental and theoretical information [21–25]. In order to preserve the WT identity, we employ the gauge-invariant form factor prescription given in Refs. [26–28]. The cutoff parameters for the form factors are determined in such a way that the experimental data are reproduced. With these parameters fixed, we compute the total (σ) and differential cross sections ($d\sigma/d\Omega$) for the $\gamma p \to K^*\Sigma$ processes. In addition, the single-polarization observables such as those for the photon-beam (Σ), target (T_y), and recoil baryon (P_y), are presented as useful theoretical guides for available and future experiments. Based on the present results, we observe that the resonance contributions play a minor role in producing the strength of the cross sections, being different from the $K^*\Lambda$ photoproduction. On the other hand, it turns out that the $\Delta(1232)$-pole diagram and K exchange in the t channel are dominant in explaining the production mechanism of $\gamma p \to K^*\Sigma$.

The present work is organized as follows: in Sec. II, we explain the general formalism of the effective Lagrangian methods and show how to fix various model parameters such as the coupling constants and the cutoff masses. The numerical results are presented and discussed in Sec. III. The last section is devoted to the summary, conclusion, and future perspectives.

II. FORMALISM

We start with the effective Lagrangian method at the tree-level Born approximation. The relevant and generic Feynman diagrams for the reaction processes $\gamma p \to K^{*0}\Sigma^+$ and $\gamma p \to K^{*+}\Sigma^0$ are shown in Fig. 1, which include N, Δ, N^*, and Δ^* poles in the s channel; the K^*, K, and κ meson exchanges in the t channel; and Λ, Σ, and $\Sigma^*(1385, 3/2^+)$ hyperons in the u channel. The contact-term contribution is necessary for satisfying the WT identity. For convenience, we assign these two production processes as the $K^{*0}\Sigma^+$ and $K^{*+}\Sigma^0$ channels, respectively, from now on. Note that, however, we do not have the K^* exchange for the $K^{*0}\Sigma^+$ channel due to their electrically neutral vertex of $\gamma K^*\bar{K}^*$ as far as we ignore the magnetic and quadratic moments of K^* as in the present work. Consequently, the contact term is also absent for the $K^{*0}\Sigma^+$ channel.

The effective Lagrangians for the Born contributions are essentially the same as those used in Refs. [16,19]. As for the photon-meson-meson interactions, we define them as follows:

$$\begin{aligned}
\mathcal{L}_{\gamma K^*K^*} &= -ie_{K^*}A^\mu(K^{*-\nu}K^{*+}_{\mu\nu} - K^{*-}_{\mu\nu}K^{*+\nu}),\\
\mathcal{L}_{\gamma K^*K} &= g_{\gamma KK^*}\varepsilon^{\mu\nu\alpha\beta}(\partial_\mu A_\nu)(\partial_\alpha K^*_\beta)\bar{K} + \text{H.c.},\\
\mathcal{L}_{\gamma K^*\kappa} &= g_{\gamma K^*\kappa}F^{\mu\nu}\bar{\kappa}K^*_{\mu\nu} + \text{H.c.},
\end{aligned} \tag{1}$$

where A_μ, K^*_μ, K, and κ denote the photon, the $K^*(892, 1^-)$, $K(495, 0^-)$, and $\kappa(800, 0^+)$, respectively [21]. The field-strength tensors for the photon and the massive vector meson are defined as $F_{\mu\nu} = \partial_\mu A_\nu - \partial_\nu A_\mu$ and $K^*_{\mu\nu} = \partial_\mu K^*_\nu - \partial_\nu K^*_\mu$, respectively. The values for the coupling constants $g_{\gamma K^*K}$ are determined from the experimental data [21], which lead to

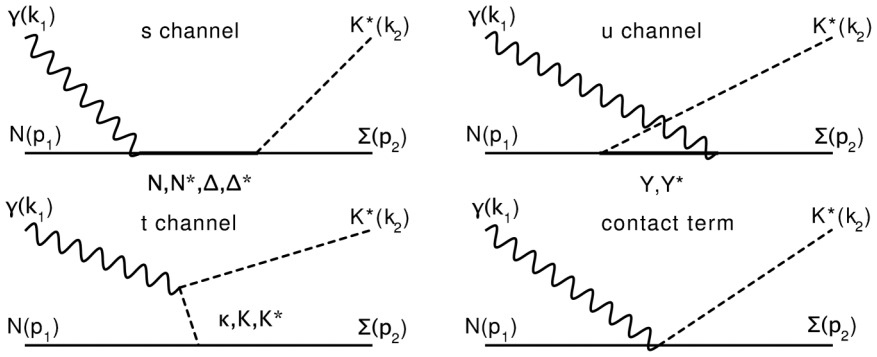

FIG. 1. Relevant Feynman diagrams for the $\gamma N \to K^*\Sigma$ reactions. N, N^*, Δ, Δ^*, Y, and Y^* denote the nucleon, nucleon resonances, delta, delta resonances, hyperons, and hyperon resonances, respectively, whereas κ, K, and K^* stand for the strange scalar, pseudoscalar, and vector mesons, respectively. The four momenta for the initial and final states are also defined, as shown in the diagrams.

$$g^{\text{charged}}_{\gamma K^* K} = 0.254\ \text{GeV}^{-1}, \qquad g^{\text{neutral}}_{\gamma K^* K} = -0.388\ \text{GeV}^{-1}, \tag{2}$$

whereas we use the vector-meson dominance model to determine the values of $g_{\gamma K^*\kappa}$ [29]:

$$g^{\text{charged}}_{\gamma K^*\kappa} = -0.119e\ \text{GeV}^{-1}, \qquad g^{\text{neutral}}_{\gamma K^*\kappa} = -2g^{\text{charged}}_{\gamma K^*\kappa}. \tag{3}$$

Here e denotes the unit electric charge $e = \sqrt{4\pi\alpha_{\text{E}}}$ with the fine-structure constant $\alpha_{\text{EM}} = 1/137.04$. As for the κ meson's parameters, we use $M_\kappa = 800$ MeV for the mass, and $\Gamma = 550$ MeV for the decay width value.

The Lagrangians for the photon-baryon-baryon interactions are written by

$$\begin{aligned}
\mathcal{L}_{\gamma NN} &= -\bar{N}\left[e_N \not{A} - \frac{e\kappa_N}{2M_N}\sigma_{\mu\nu}\partial^\nu A^\mu\right]N, \\
\mathcal{L}_{\gamma N\Delta} &= e\bar{\Delta}_\mu\left[\frac{ig_1}{2M_N}\gamma_\nu\gamma_5 + \frac{g_2}{(2M_N)^2}\gamma_5\partial_\nu\right]NF^{\mu\nu} + \text{H.c.}, \\
\mathcal{L}_{\gamma\Sigma\Sigma} &= -\bar{\Sigma}\left[e_\Sigma \not{A} - \frac{e\kappa_\Sigma}{2M_N}\sigma_{\mu\nu}\partial^\nu A^\mu\right]\Sigma,
\end{aligned} \tag{4}$$

where N, Σ, and Δ stand for the nucleon, $\Sigma(1193, 1/2^+)$, and $\Delta(1232, 3/2^+)$, respectively, and M_N denotes the mass of the nucleon. Here κ_B represents the anomalous magnetic moment of the baryon B. The corresponding PDG values [21] are given as

$$\begin{aligned}
&\kappa_n = -1.91, \qquad \kappa_p = +1.79, \qquad \kappa_{\Sigma^-} = -0.16, \\
&\kappa_{\Sigma^0} = +0.65, \qquad \kappa_{\Sigma^+} = +1.46.
\end{aligned} \tag{5}$$

The Δ field with spin-3/2 is described by the Rarita-Schwinger formalism [30,31]. We choose the electric and magnetic couplings as $g_1 = 4.13$ and $g_2 = 4.74$ using the experimental data for the helicity amplitudes [21,22].

We define the effective Lagrangians for the meson-baryon-baryon Yukawa interactions as follows:

$$\begin{aligned}
\mathcal{L}_{K^*N\Sigma} &= -g_{K^*N\Sigma}\left[\bar{K}^{*\mu}\bar{\Sigma}\gamma_\mu - \frac{\kappa_{K^*N\Sigma}}{2M_N}\partial^\nu\bar{K}^{*\mu}\bar{\Sigma}\sigma_{\mu\nu}\right]N \\
&\quad + \text{H.c.}, \\
\mathcal{L}_{KN\Sigma} &= -ig_{KN\Sigma}\bar{K}\,\bar{\Sigma}\,\gamma_5 N + \text{H.c.}, \\
\mathcal{L}_{\kappa N\Sigma} &= -g_{\kappa N\Sigma}\bar{\kappa}\,\bar{\Sigma}\,N + \text{H.c.}, \\
\mathcal{L}_{K^*\Delta\Sigma} &= -\frac{if_{K^*\Delta\Sigma}}{2M_{K^*}}\bar{\Delta}^\mu\gamma^\nu\gamma_5\Sigma K^*_{\mu\nu} + \text{H.c.},
\end{aligned} \tag{6}$$

where $\Sigma = \boldsymbol{\tau}\cdot\boldsymbol{\Sigma}$ in which $\boldsymbol{\tau}$ indicate the Pauli matrices. The isospin structures of the Δ vertices in Eqs. (4) and (6) are given as follows, respectively:

$$\bar{\Delta} I^0 N, \qquad \bar{\Delta}\boldsymbol{I}\cdot\boldsymbol{\Sigma}K^*, \tag{7}$$

where $\boldsymbol{I}$ stands for the isospin transition $(3/2 \to 1/2)$ matrices

$$I^- = \frac{1}{\sqrt{6}}\begin{pmatrix} 0 & 0 \\ 0 & 0 \\ \sqrt{2} & 0 \\ 0 & \sqrt{6} \end{pmatrix}, \qquad I^0 = \frac{1}{\sqrt{6}}\begin{pmatrix} 0 & 0 \\ 2 & 0 \\ 0 & 2 \\ 0 & 0 \end{pmatrix},$$
$$I^+ = \frac{1}{\sqrt{6}}\begin{pmatrix} \sqrt{6} & 0 \\ 0 & \sqrt{2} \\ 0 & 0 \\ 0 & 0 \end{pmatrix}. \tag{8}$$

The strong coupling constants for the meson and octet baryons can be estimated by the Nijmegen soft-core model (NSC97a) [23], and the corresponding values are presented by

$$g_{K^*N\Sigma} = -2.46, \qquad \kappa_{K^*N\Sigma} = -0.47, \qquad g_{\kappa N\Sigma} = -5.32, \tag{9}$$

whereas we estimate the value of $f_{K^*\Delta\Sigma}$ using the quark-model prediction and SU(3) flavor symmetry relation:

$$f_{K^*\Delta\Sigma} = -\frac{2M_{K^*}}{M_\rho}f_{\rho N\Delta} = -12.8, \tag{10}$$

with $f_{\rho N\Delta} = 5.5$ [32]. The value of $g_{KN\Sigma}$ is also obtained by using a similar relation, which gives $g_{KN\Sigma} = 3.58$.

Now, we are in a position to consider the resonance contributions. First, we write the EM and strong effective Lagrangians with the hyperon resonance Σ^*:

$$\begin{aligned}
\mathcal{L}_{\gamma\Sigma\Sigma^*} &= e\bar{\Sigma}^*_\mu\left[\frac{ig^V_{\gamma\Sigma\Sigma^*}}{2M_N}\gamma_\nu\gamma_5 + \frac{g^T_{\gamma\Sigma\Sigma^*}}{(2M_N)^2}\gamma_5\partial_\nu\right]\Sigma F^{\mu\nu} + \text{H.c.}, \\
\mathcal{L}_{K^*N\Sigma^*} &= i\frac{f^{(1)}_{K^*N\Sigma^*}}{2M_{K^*}}\bar{N}\gamma^\nu\gamma_5\Sigma^{*\mu}K^*_{\mu\nu} \\
&\quad + \frac{f^{(2)}_{K^*N\Sigma^*}}{(2M_{K^*})^2}\partial^\nu\bar{N}\gamma_5\Sigma^{*\mu}K^*_{\mu\nu} \\
&\quad - \frac{f^{(3)}_{K^*N\Sigma^*}}{(2M_{K^*})^2}\bar{N}\gamma_5\Sigma^{*\mu}\partial^\nu K^*_{\mu\nu} + \text{H.c.}
\end{aligned} \tag{11}$$

In order to determine $g^{V,T}_{\gamma\Sigma\Sigma^*}$, we need to know the experimental data for the $\Sigma^* \to \Sigma\gamma$ radiative decay. However, only the upper limits of the hyperon decay rates are known [33]. Moreover, $\Sigma^{*-} \to \Sigma^-\gamma$ is known to be U-spin forbidden, which means its decay rate vanishes in the exact SU(3) symmetry. On the other hand, these decay rates were predicted within several different theoretical frameworks [34–39]. Since Ref. [38] has computed the hyperon radiative decay rates as well as the $E2/M1$ ratio, we use the results of Ref. [38], so that we are able to extract $g^{V,T}_{\gamma\Sigma\Sigma^*}$ as follows:

TABLE I. Parameters for the resonances in Eqs. (13) and (15). The decay amplitudes $G(s, l)$ are computed from Ref. [25]. The full decay widths Γ_R [MeV] and helicity amplitudes $A_{1,3}$ [GeV$^{-\frac{1}{2}}$] are taken from the experimental data [21] and theoretical estimations [24]. The $(+, -)$ sign of g_1 for S_{11} corresponds to its decay to $(K^{*0}\Sigma^+, K^{*+}\Sigma^0)$.

	Resonance	$G_{s,l}$	g_1	Γ_R	A_1	A_3	h_1	h_2
N^*	$D_{13}(2080)$	-0.5	-0.238	300	-0.020	$+0.017$	$+0.608$	-0.620
	$S_{11}(2090)$	-0.9	∓ 0.909	300	$+0.012$	$\cdots$	$+0.055$	$\cdots$
	$G_{17}(2190)$	-0.3	$+5.63$	300	-0.034	$+0.028$	$+7.69$	-7.17
	$D_{15}(2200)$	$+0.2$	$+1.11$	300	-0.002	-0.006	$+0.123$	$+0.011$
Δ^*	$S_{31}(2150)$	-4.8	$+2.54$	300	$+0.004$	$\cdots$	$+0.018$	$\cdots$
	$G_{37}(2200)$	$+0.5$	± 8.32	300	$+0.014$	-0.004	-2.31	$+2.47$
	$F_{37}(2390)$	$+0.6$	$+5.02$	300	$+0.024$	$+0.030$	-1.89	-1.54
Y^*	$\Sigma^*(1385, 3/2^+)$	$\cdots$	$\cdots$	$\cdots$	$\cdots$	$\cdots$	$\cdots$	$\cdots$

$$
\begin{aligned}
g^{V+}_{\gamma\Sigma\Sigma^*} &= +2.66, & g^{T+}_{\gamma\Sigma\Sigma^*} &= +0.74,\\
g^{V0}_{\gamma\Sigma\Sigma^*} &= +1.10, & g^{T0}_{\gamma\Sigma\Sigma^*} &= +0.55,\\
g^{V-}_{\gamma\Sigma\Sigma^*} &= +0.49, & g^{T-}_{\gamma\Sigma\Sigma^*} &= -0.39.
\end{aligned} \tag{12}
$$

The coupling constant $f^{(1)}_{K^*N\Sigma^*}$ can be determined to be -5.21 by flavor SU(3) symmetry. Because of the lack of experimental and theoretical information on $f^{(2,3)}_{K^*N\Sigma^*}$, we do not consider them for brevity in the present work.

In addition to the hyperon resonances, we now include the s-channel resonance contributions. Here, we consider the $D_{13}(2080)$, $S_{11}(2090)$, $G_{17}(2190)$, and $D_{15}(2200)$ for the nucleon and $S_{31}(2150)$, $G_{37}(2200)$, and $F_{37}(2390)$ for the delta resonances, which are located near the threshold of $K^*\Sigma$ photoproduction. The relevant EM Lagrangians for those baryon resonances can be written as

$$
\begin{aligned}
\mathcal{L}_{\gamma NR_{1/2^\pm}} &= \frac{eh_1}{2M_N}\bar{N}\Gamma^{(\mp)}\sigma_{\mu\nu}\partial^\nu A^\mu R + \text{H.c.},\\
\mathcal{L}_{\gamma NR_{3/2^\pm}} &= -ie\left[\frac{h_1}{2M_N}\bar{N}\Gamma^{(\pm)}_\nu - \frac{ih_2}{(2M_N)^2}\partial_\nu\bar{N}\Gamma^{(\pm)}\right]F^{\mu\nu}R_\mu\\
&\quad + \text{H.c.},\\
\mathcal{L}_{\gamma NR_{5/2^\pm}} &= e\left[\frac{h_1}{(2M_N)^2}\bar{N}\Gamma^{(\mp)}_\nu - \frac{ih_2}{(2M_N)^3}\partial_\nu\bar{N}\Gamma^{(\mp)}\right]\partial^\alpha F^{\mu\nu}R_{\mu\alpha}\\
&\quad + \text{H.c.},\\
\mathcal{L}_{\gamma NR_{7/2^\pm}} &= ie\left[\frac{h_1}{(2M_N)^3}\bar{N}\Gamma^{(\pm)}_\nu - \frac{ih_2}{(2M_N)^4}\partial_\nu\bar{N}\Gamma^{(\pm)}\right]\\
&\quad \times \partial^\alpha\partial^\beta F^{\mu\nu}R_{\mu\alpha\beta} + \text{H.c.},
\end{aligned} \tag{13}
$$

where R stands for the field corresponding to the nucleon and delta resonances $R = (N^*, \Delta^*)$ with spin and parity given. $\Gamma^{(\pm)}$ and $\Gamma^{(\pm)}_\nu$ in Eq. (13) are defined as

$$
\Gamma^{(\pm)} = \begin{pmatrix}\gamma_5\\ \mathbf{1}\end{pmatrix}, \qquad \Gamma^{(\pm)}_\mu = \begin{pmatrix}\gamma_\mu\gamma_5\\ \gamma_\mu\end{pmatrix}. \tag{14}
$$

The coupling constants are determined by using the experimental data for the helicity amplitudes [21,22] and the quark-model predictions of Ref. [22,24]. Those for the strong interactions are given as

$$
\begin{aligned}
\mathcal{L}_{K^*\Sigma R_{1/2^\pm}} &= -\frac{1}{2M_N}\bar{R}\Bigg[g_1\left(\pm\frac{\Gamma^{(\mp)}_\mu\Sigma\partial^2}{M_R \mp M_N} - i\Gamma^{(\mp)}\partial_\mu\right)\\
&\quad - g_2\Gamma^{(\mp)}\sigma_{\mu\nu}\Sigma\partial^\nu\Bigg]K^{*\mu} + \text{H.c.},\\
\mathcal{L}_{K^*\Sigma R_{3/2^\pm}} &= i\bar{R}_\mu\Bigg[\frac{g_1}{2M_N}\Sigma\Gamma^{(\pm)}_\nu \mp \frac{ig_2}{(2M_N)^2}\partial_\nu\Sigma\Gamma^{(\pm)}\\
&\quad \pm \frac{ig_3}{(2M_N)^2}\Sigma\Gamma^{(\pm)}\partial_\nu\Bigg]K^{*\mu\nu} + \text{H.c.},\\
\mathcal{L}_{K^*\Sigma R_{5/2^\pm}} &= \bar{R}_{\mu\alpha}\Bigg[\frac{g_1}{(2M_N)^2}\Sigma\Gamma^{(\mp)}_\nu \pm \frac{ig_2}{(2M_N)^3}\partial_\nu\Sigma\Gamma^{(\mp)}\\
&\quad \mp \frac{ig_3}{(2M_N)^3}\Sigma\Gamma^{(\mp)}\partial_\nu\Bigg]\partial^\alpha K^{*\mu\nu} + \text{H.c.},\\
\mathcal{L}_{K^*\Sigma R_{7/2^\pm}} &= -i\bar{R}_{\mu\alpha\beta}\Bigg[\frac{g_1}{(2M_N)^3}\Sigma\Gamma^{(\pm)}_\nu \mp \frac{ig_2}{(2M_N)^4}\partial_\nu\Sigma\Gamma^{(\pm)}\\
&\quad \pm \frac{ig_3}{(2M_N)^4}\Sigma\Gamma^{(\pm)}\partial_\nu\Bigg]\partial^\alpha\partial^\beta K^{*\mu\nu} + \text{H.c.},
\end{aligned} \tag{15}
$$

where M_R is the corresponding resonance mass. The strong coupling constants in Eq. (15) can be determined from the theoretical estimations for the partial-wave decay amplitudes [25]:

$$
\Gamma_{R\to K^*\Sigma} = \sum_{s,l}|G(s, l)|^2, \tag{16}
$$

where $\Gamma_{R\to K^*\Sigma}$ is the decay width of $R \to K^*\Sigma$. The values for the partial-wave coupling strengths $G(s, l)$ can be found in Ref. [25]. Since the purpose of the present work is to investigate the role of resonances near the threshold, it is enough to take into account the contributions of the lower partial waves. Hence, we consider only the g_1 terms in Eq. (15), employing only the lowest partial-wave contribution for $G(s, l)$. Using Eq. (16) and the prediction of Ref. [25], we then can compute the strong coupling constants for the resonances. The signs of these strong coupling constants are determined by fitting the experimental data [12,14], as will be shown in the next section. We list all the parameters of the resonances in Table I.

The form factors are included in a gauge-invariant manner, so that the invariant amplitudes can be expressed as

TABLE II. Cutoff masses for the form factors in Eq. (19) for each channel.

Λ_Φ for t channel			Λ_B for s channel				Λ_B for u channel		
Λ_{K^*}	Λ_K	Λ_κ	Λ_N	Λ_Δ	Λ_{N^*}	Λ_{Δ^*}	Λ_Λ	Λ_Σ	Λ_{Σ^*}
0.80 GeV	1.15 GeV	1.15 GeV	1.50 GeV	1.50 GeV	1.00 GeV	1.00 GeV	0.70 GeV	0.95 GeV	0.95 GeV

$$\mathcal{M} = [\mathcal{M}^{\rm elec}_{s(N)} + \mathcal{M}_{u(\Sigma)}]F^2_{\rm com} + \mathcal{M}^{\rm mag}_{s(N)}F^2_N + \mathcal{M}_{t(K)}F^2_K + \mathcal{M}_{t(\kappa)}F^2_\kappa + \mathcal{M}_{s(\Delta)}F^2_\Delta + \mathcal{M}_{u(\Sigma^*)}F^2_{\Sigma^*} + \mathcal{M}_{s(N^*)}F^2_{N^*} + \mathcal{M}_{s(\Delta^*)}F^2_{\Delta^*} \quad (17)$$

for the $K^{*0}\Sigma^+$ channel and

$$\mathcal{M} = [\mathcal{M}_{t(K^*)} + \mathcal{M}^{\rm elec}_{s(N)} + \mathcal{M}_{\rm c}]F^2_{\rm com} + \mathcal{M}^{\rm mag}_{s(N)}F^2_N + \mathcal{M}_{t(K)}F^2_K + \mathcal{M}_{t(\kappa)}F^2_\kappa + \mathcal{M}_{s(\Delta)}F^2_\Delta + \mathcal{M}_{u(\Lambda)}F^2_\Lambda + \mathcal{M}_{u(\Sigma)}F^2_\Sigma + \mathcal{M}_{u(\Sigma^*)}F^2_{\Sigma^*} + \mathcal{M}_{s(N^*)}F^2_{N^*} + \mathcal{M}_{s(\Delta^*)}F^2_{\Delta^*} \quad (18)$$

for the $K^{*+}\Sigma^0$ channel, respectively. The explicit expressions for each invariant amplitude can be found in the Appendix. The common form factor $F_{\rm com}$ and those for the off-mass shell meson (Φ) and baryon (B) vertices are written generically as

$$F_{\rm com} = F_N F_{\Sigma(K^*)} - F_N - F_{\Sigma(K^*)}, \qquad F_\Phi = \frac{\Lambda^2_\Phi - M^2_\Phi}{\Lambda^2_\Phi - q^2},$$
$$F_B = \frac{\Lambda^4_B}{\Lambda^4_B + (q^2 - M^2_B)^2}, \quad (19)$$

where q denotes the off-shell momentum of the relevant hadron in each kinematic channel [26–28]. For the mesonic ($\Phi = \kappa$, K, K^*) and baryonic ($B = N$, Δ, Λ, Σ, Σ^*, R) vertices, we consider different types of form factors with the cutoff masses Λ_Φ and Λ_B.

III. NUMERICAL RESULTS

In this section, we present and discuss the numerical results. All the calculations are performed in the center-of-mass (CM) frame. The cutoff masses for the phenomenological form factors in Eq. (19) are determined to reproduce the experimental data for the total and differential cross sections for the $K^{*0}\Sigma^+$ channel from the CBELSA/TAPS [12] and CLAS [14] collaborations. The determined cutoff masses are listed in Table II.

We draw the numerical results for the total cross sections for the $K^{*0}\Sigma^+$ channel in the left panel of Fig. 2 in which the K-exchange, κ-exchange, and Δ-pole contributions are depicted in dot-dot-dashed, dash-dash-dotted, and dot-dashed curves, separately. The solid one designates the total cross section with all contributions included. The black circles denote the CBELSA/TAPS [12] data. We estimate the total cross sections from the CLAS data [14] for the differential cross sections, which are represented by the open squares, based on the interpolating polynomial method to the fourth order. Our result shown by the solid line is in a good agreement with the CBELSA/TAPS data up to around $E_\gamma \sim 2.1$ GeV. While the present results seem to be underestimated as E_γ increases, they are found to be closer to the estimation from the CLAS data. We have tried to reproduce the CLAS data rather than those of CBELSA/TAPS because there exists more experimental information for the wider photon energy region, $E_\gamma = (1.925\text{–}2.9125)$. It turns out that the K exchange and the $\Delta(1232)$-pole contributions can only describe the experimental data for the $\gamma p \to K^{*0}\Sigma^+$ total cross section, as shown in the dashed curve, which indicates that the baryon-resonance contributions are almost negligible.

In the right panel of Fig. 2, we show the results of the total cross section for the $\gamma p \to K^{*+}\Sigma^0$ process. Note that its production strength is a little smaller than that of the

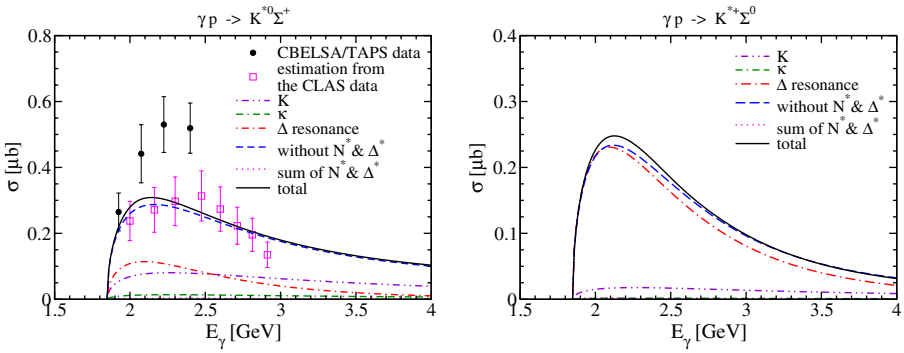

FIG. 2 (color online). Total cross sections for $\gamma p \to K^{*0}\Sigma^+$ as functions of the photon energy E_γ in the left panel. The black circles denote the CBELSA/TAPS data [12], whereas the open squares represent the estimated values extracted from the CLAS data [14]. The total cross sections for $\gamma p \to K^{*+}\Sigma^0$ are given in the right panel with the same notation.

$\gamma p \to K^{*0}\Sigma^+$ one. Though the isospin factor of the $K^{*+}\Sigma^0\Delta^+$ vertex is larger than that of the $K^{*0}\Sigma^+\Delta^+$ one, i.e., $I_{K^{*+}\Sigma^0\Delta^+}/I_{K^{*0}\Sigma^+\Delta^+} = \sqrt{2}$, the t channel plays a prominent role in the $K^{*0}\Sigma^+$ process compared with the $K^{*+}\Sigma^0$ one, as shown in Fig. 2. The other N^*, Δ^*, and hyperon resonances have minute effects on the $K^{*+}\Sigma^0$ production, similar to the $K^{*0}\Sigma^+$ one. Thus, all other resonances except for $\Delta(1232)$ seem to be unimportant in describing the *unpolarized* cross sections for $K^*\Sigma$ photoproduction. However, even though these resonance contributions are negligibly small, we will see later that they play certain roles in the polarization observables. In particular, they exhibit more sensitive angular dependence than other contributions. These features are obviously distinguished from the $K^*\Lambda$ photoproduction previously examined in Ref. [19]. We also verified that with a different set of the strong coupling constants, such as those from the Nijmegen potential (NSC97f) [23], we reached the same conclusion.

Since the N^* and Δ^* resonances have effects on the polarization observables as we have mentioned already, it is necessary to scrutinize them. In Fig. 3, we draw each contribution of the N^* [$D_{13}(2080)$, $S_{11}(2090)$, $G_{17}(2190)$] and Δ^* [$S_{31}(2150)$, $F_{37}(2390)$] resonances to the total cross section. Though we computed the contributions of the $D_{15}(2200)$ and $G_{37}(2200)$, we did not show them in Fig. 3, because they are almost negligible. As expected, the magnitude of the resonance contributions is about 100 times smaller than that of the Born term contributions. This feature of higher N^* and Δ^* resonances is very different from the case of $K^*\Lambda$ photoproduction [19], which ensues from the fact that the strong coupling constants of Σ to these resonances are much smaller than those of Λ to them, according to the SU(6) quark-model calculations [25]. Explicitly comparing Table I in this work with Table III in Ref. [19], one can verify, for example, $g_{K^*\Sigma D_{13}}/g_{K^*\Lambda D_{13}} \sim 1/7$ due to the different isospin factors.

Figure 4 depicts the numerical results for the differential cross sections $d\sigma/d\cos\theta$ for the $K^{*0}\Sigma^+$ channel as functions of $\cos\theta$. The experimental data are taken from the CBELSA/TAPS [12] (black circle) and CLAS [14] (open square) collaborations measured in the range of the photon energy $E_\gamma = (1.925\text{–}2.9125)$ GeV. Note that there is almost no effect from other N^* and Δ^* resonances, but our total results reproduce the data qualitatively well. Theoretically, the t-channel contributions such as κ and K exchanges enhance the differential cross section in the forward direction. Although we did not show it explicitly in the present work, we checked that K^* exchange did not contribute to the results in the forward direction. We note that the Δ-pole and u-channel Born contributions are responsible for the enhancement in the backward angle.

We also illustrate the differential cross sections for the $\gamma p \to K^{*+}\Sigma^0$ process in Fig. 5 in the same manner as in Fig. 4. As understood from Fig. 2, the overall strengths of the differential cross sections are smaller than those of the $K^{*0}\Sigma^+$ channel. Since there are the K^* exchange, the Λ exchange, and the contact term, in addition to other diagrams so as to satisfy the WT identity, the angular dependence of the differential cross sections for $K^{*+}\Sigma^0$ photoproduction turns out to be rather different from those for $K^{*0}\Sigma^+$. Though there is some t-channel contribution to the differential cross section in the forward direction, the Δ exchange becomes dominant.

We are now in a position to discuss the single-polarization observables. The photon-beam Σ_γ, recoil P_y, and target T_y asymmetries are defined as follows [40]:

$$\Sigma_\gamma \equiv \frac{d\sigma(\epsilon_\perp) - d\sigma(\epsilon_\parallel)}{d\sigma_{\rm unpol}},$$
$$P_y \equiv \frac{d\sigma(s_y^\Sigma = \frac{1}{2}) - d\sigma(s_y^\Sigma = -\frac{1}{2})}{d\sigma_{\rm unpol}}, \tag{20}$$
$$T_y \equiv \frac{d\sigma(s_y^N = \frac{1}{2}) - d\sigma(s_y^N = -\frac{1}{2})}{d\sigma_{\rm unpol}},$$

where $d\sigma_{\rm unpol}$ stands for the unpolarized differential cross section. These polarization observables satisfy the following conditions in the collinear limit:

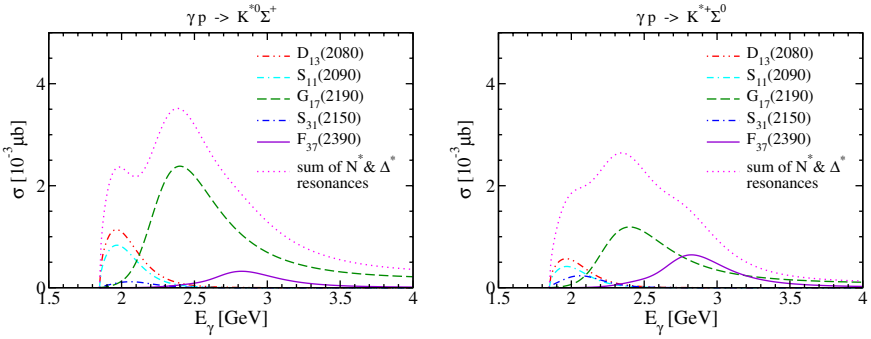

FIG. 3 (color online). N^* and Δ^* resonance contributions to the total cross sections for $\gamma p \to K^{*0}\Sigma^+$ as functions of the photon energy E_γ in the left panel and for $\gamma p \to K^{*+}\Sigma^0$ in the right panel with the same notation, respectively.

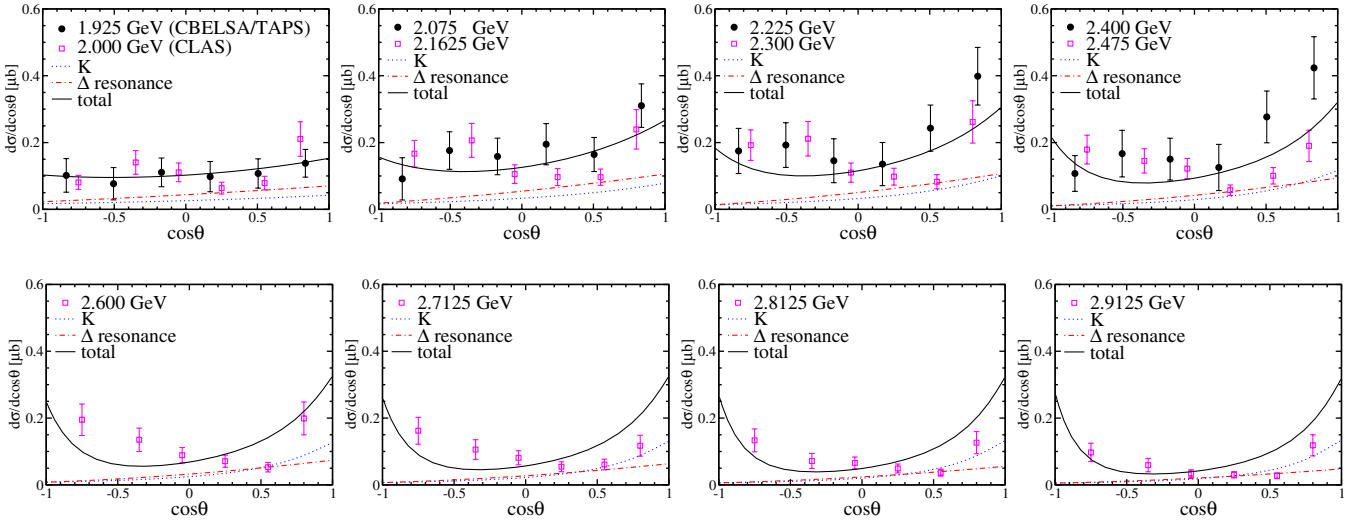

FIG. 4 (color online). Differential cross sections for $\gamma p \to K^{*0}\Sigma^+$ as functions of $\cos\theta$ for different photon energies (E_γ) in the range (1.925–2.9125) GeV. The dotted curve shows the t-channel effects (K and κ exchanges), whereas the dot-dashed one draws the Δ-pole contribution. The solid one represents the total result. The experimental data of the CBELSA/TAPS and CLAS collaborations are taken from Refs. [12,14], respectively.

$$\Sigma_\gamma = P_y = T_y = 0 \quad \text{at} \quad \cos\theta = \pm 1. \tag{21}$$

Throughout the present work, we define the reaction plane by the x-z axes. Thus, the y axis is perpendicular to the reaction plane. The photon polarization vectors $\epsilon_\perp$ and $\epsilon_\parallel$ are defined in the Appendix, while s_y^B indicates the spin of a baryon B along the y direction.

In Fig. 6, we depict the numerical results of Σ_γ for $K^{*0}\Sigma^+$ in the upper panel and for $K^{*+}\Sigma^0$ in the lower panel as functions of $\cos\theta$ in the range of $E_\gamma =$ (2.075–2.9125) GeV. It is found that the N^* and Δ^* resonances do not much affect the Σ_γ for both $K^{*+}\Sigma^0$ and $K^{*0}\Sigma^+$ photoproductions, which was already seen for the differential cross sections as shown in Figs. 4 and 5. While κ and K exchanges govern the $K^{*0}\Sigma^+$ production mechanism because of their large magnetic couplings, the Δ-pole contribution in the s channel pulls down Σ_γ to the negative direction. The effect of the Δ-pole contribution becomes larger as E_γ increases. The dependence of Σ_γ on $\cos\theta$ is more complicated in the case of the $K^{*+}\Sigma^0$ production, in particular, for higher E_γ, as illustrated in the lower panel of Fig. 6.

In the upper panel of Fig. 7, we draw the photon-beam asymmetries for $K^{*0}\Sigma^+$ photoproduction with and without N^* and Δ^* resonances in order as functions of E_γ, the scattering angle being varied between $\theta = 0°$ and

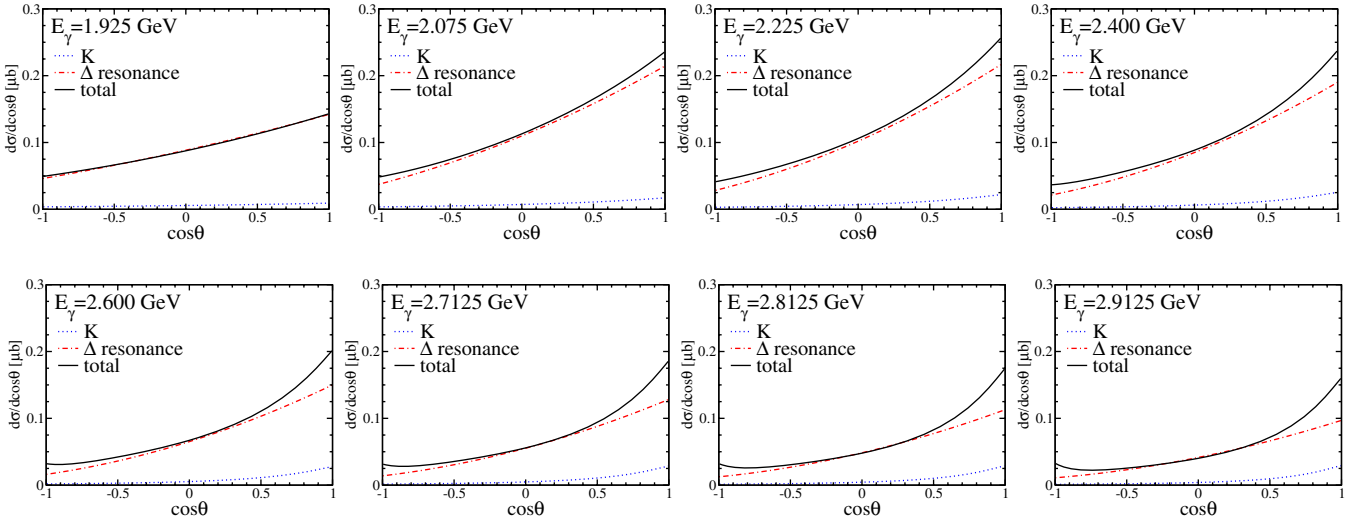

FIG. 5 (color online). Differential cross sections for $\gamma p \to K^{*+}\Sigma^0$ as functions of $\cos\theta$ for different photon energies (E_γ) in the range (1.925–2.9125) GeV. The dotted curve shows the t-channel effects (K and κ exchanges), whereas the dot-dashed one draws the Δ-pole contribution. The solid one represents the total result.

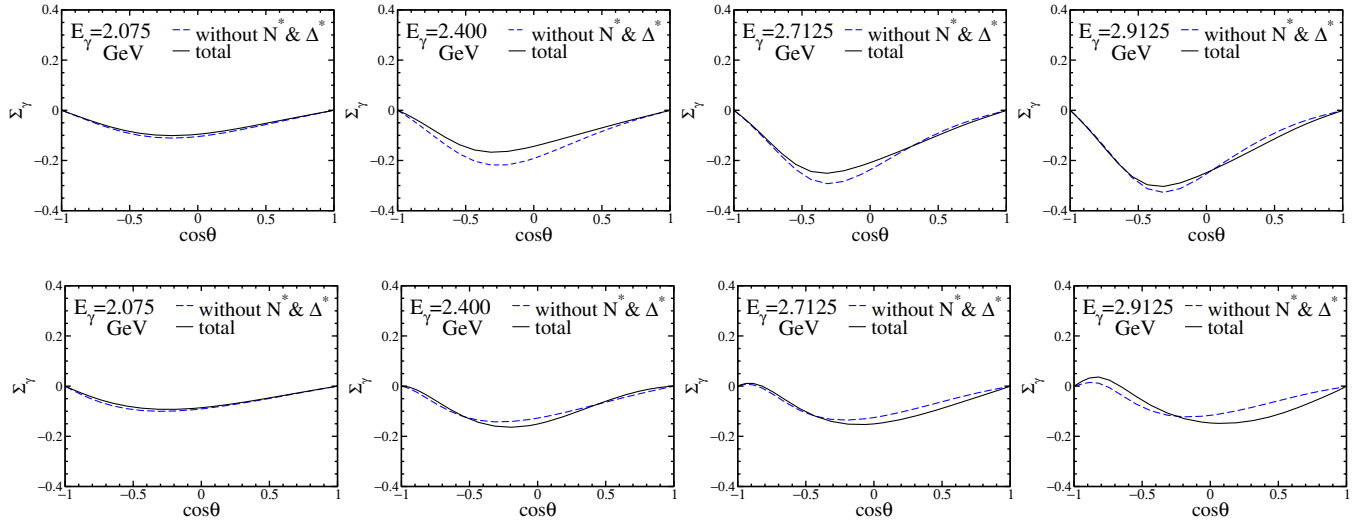

FIG. 6 (color online). In the upper panel, photon-beam asymmetry Σ_γ for $\gamma p \to K^{*0}\Sigma^+$ as functions of $\cos\theta$ in the range of $E_\gamma = (2.075\text{–}2.9125)$ GeV. The solid and dashed curves represent the results with and without the resonance contributions, respectively. In the lower panel, photon-beam asymmetry Σ_γ for $\gamma p \to K^{*+}\Sigma^0$ with the same notation.

$\theta = 180°$. In the lower panel, Σ_γ for the $K^{*+}\Sigma^0$ channel is depicted in the same notation as the $\gamma p \to K^{*0}\Sigma^+$ process. Though the effects of the N^* and Δ^* resonances seem to be small, one can see a slight change of Σ_γ as E_γ increases. In particular, the influence of the higher resonances is more clearly revealed in the intermediate angles ($60° \lesssim \theta \lesssim 120°$), in the case of the $K^{*+}\Sigma^0$ channel.

In the upper panel of Fig. 8, the recoil asymmetries P_y for $\gamma p \to K^{*0}\Sigma^+$ are presented as functions of $\cos\theta$ in the range of the photon energy $E_\gamma = (2.075\text{–}2.9125)$ GeV. The solid and dashed curves illustrate the results of P_y with and without the N^* and Δ^* resonances. We observe that the higher resonances have some effects on P_y, in contradiction to the case of Σ_γ. Since those resonances we have considered have rather large spins, their effects on

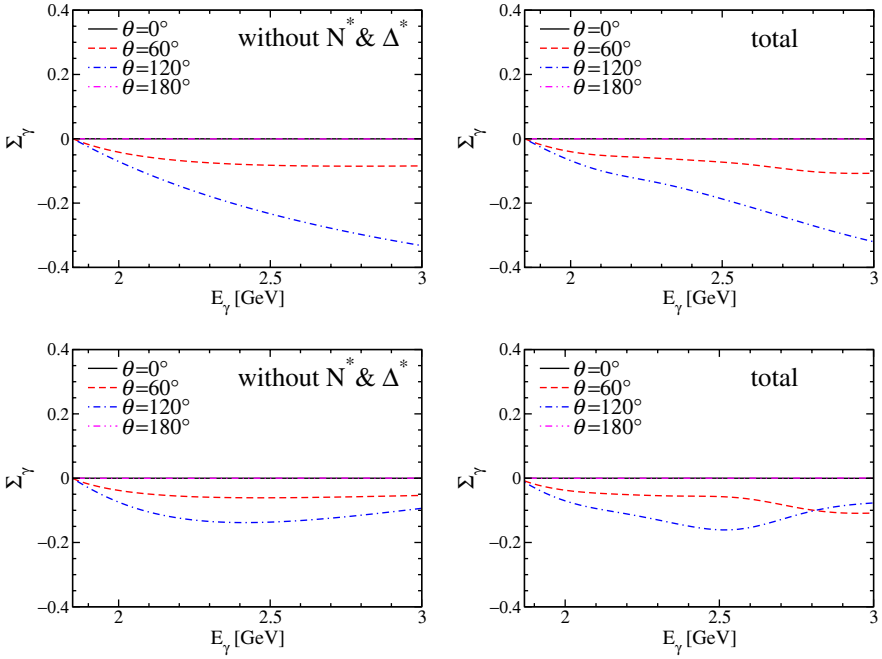

FIG. 7 (color online). In the upper panel, photon-beam asymmetries Σ_γ for $\gamma p \to K^{*0}\Sigma^+$ with and without N^* and Δ^* resonances are drawn in order as functions of the photon energy E_γ, the scattering angle being changed from 0° to 180°. In the lower panel, those for $\gamma p \to K^{*+}\Sigma^0$ are shown with and without the resonance contributions, respectively.

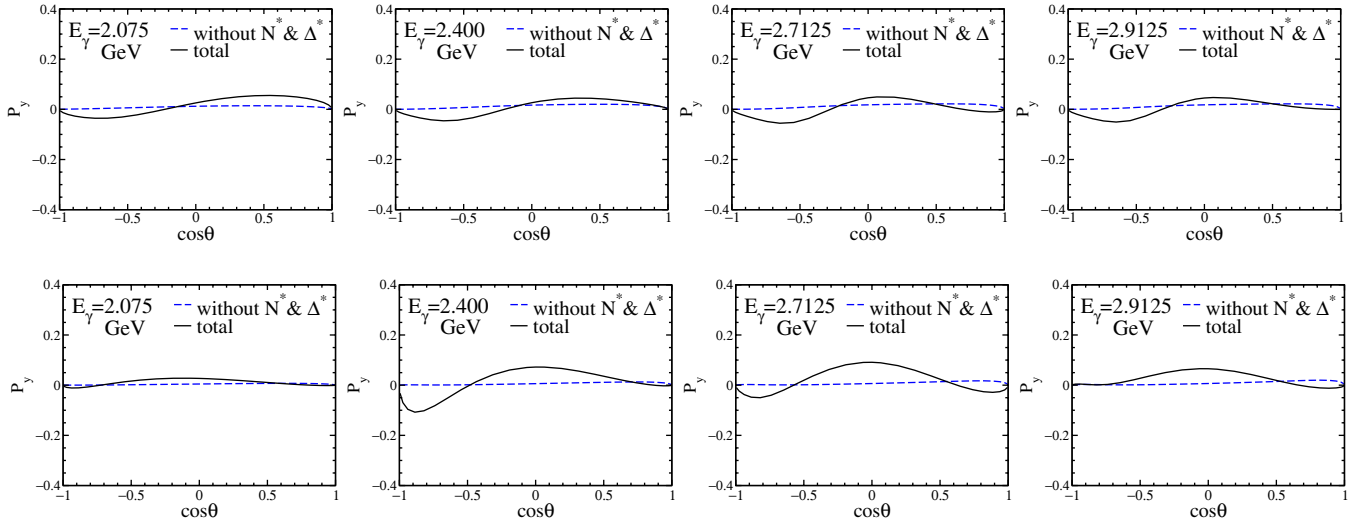

FIG. 8 (color online). Recoil asymmetries P_y for $K^*\Sigma$ photoproduction as functions of $\cos\theta$ in the range of the photon energy $E_\gamma = 2.075$–2.9125 GeV. In the upper and lower panels, P_y is drawn for the $K^{*0}\Sigma^+$ and $K^{*+}\Sigma^0$ productions, respectively. The solid and dashed curves stand for the results with and without the N^* and Δ^* resonances, respectively.

recoil and target asymmetries defined as the subtraction between the polarized differential cross sections with opposite spin directions of the baryons involved are expected to be natural. Moreover, the contributions of the N^* resonances are amplified as E_γ increases, as shown in the upper panel of Fig. 8. In the lower panel of Fig. 8, P_y for $K^{*+}\Sigma^0$ photoproduction is depicted. In this case, the effects of the higher resonances are mild in the lower E_γ region. However, as E_γ increases, P_y starts to show again some dependence on the scattering angle.

Figure 9 draws P_y as functions of E_γ for the $K^{*0}\Sigma^+$ channel in the upper panel with and without the N^* and Δ^* resonances in order and for the $K^{*+}\Sigma^0$ channel in the lower one in the same way. The scattering angle is changed from 0° to 180°. When the higher resonances are turned off, P_y is in general almost independent of E_γ. However, including

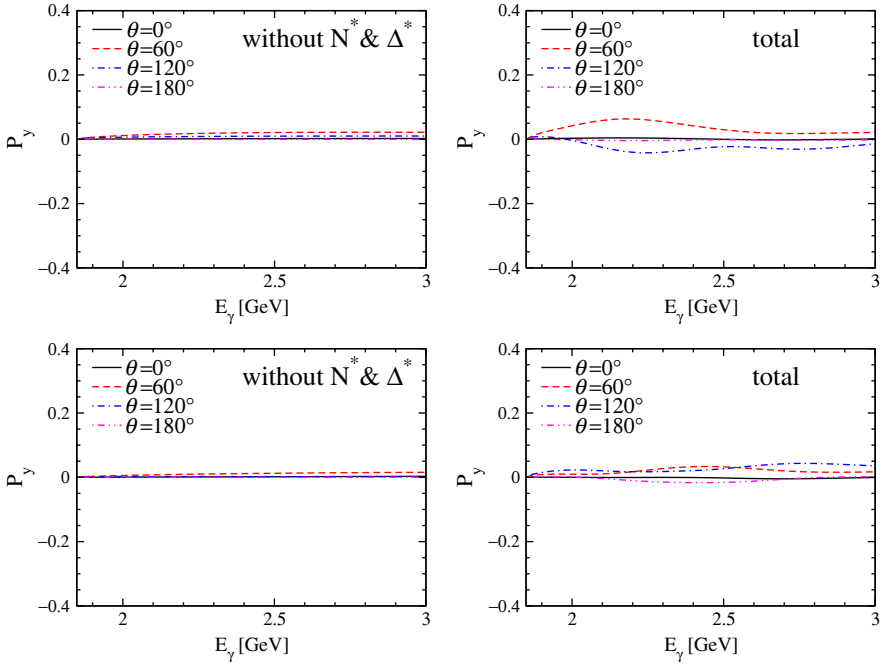

FIG. 9 (color online). In the upper panel, recoil asymmetries P_y for $\gamma p \to K^{*0}\Sigma^+$ with and without N^* and Δ^* resonances are drawn in order as functions of the photon energy E_γ, the scattering angle being changed from 0° to 180°. In the lower panel, those for $\gamma p \to K^{*+}\Sigma^0$ are shown with and without the resonance contributions, respectively.

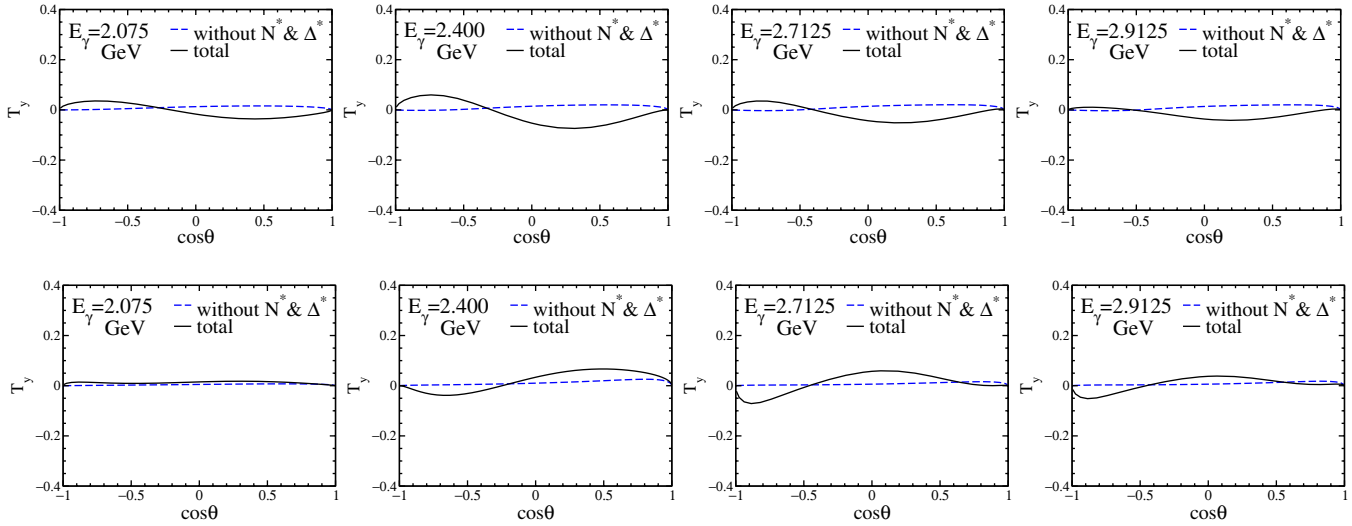

FIG. 10 (color online). Target asymmetries T_y for $K^*\Sigma$ photoproduction as functions of $\cos\theta$ in the range of the photon energy $E_\gamma = (2.075\text{–}2.9125)$ GeV. In the upper and lower panels, T_y are drawn for the $K^{*0}\Sigma^+$ and $K^{*+}\Sigma^0$ productions, respectively. The solid and dashed curves stand for the results with and without the N^* and Δ^* resonances, respectively.

the higher resonances, we find that P_y at $\theta = 60°$ for the $K^{*0}\Sigma^+$ channel starts to rise until $E_\gamma \approx 2.2$ GeV and then falls off slowly, as E_γ increases. On the other hand, P_y at $\theta = 60°$ for the $K^{*+}\Sigma^0$ channel begins to increase around 2.1 GeV and then saturates around 2.5 GeV.

Finally, we provide the numerical results for the target asymmetries T_y in Fig. 10 as functions of $\cos\theta$ in the same manner as in Fig. 8. As shown in Fig. 10, the effects of the higher resonances on T_y tend to be very similar to those on P_y. Interestingly, however, we find that the phases of the T_y curves for the $K^{*0}\Sigma^+$ and $K^{*+}\Sigma^0$ are opposite to each other. The dependence of T_y on E_γ is shown in Fig. 11 in the same way as Fig. 9. Again, it turns out that the higher resonance contributions become obvious around $E_\gamma = (2.0 \sim 2.5)$ GeV, due to the similar reason for P_y.

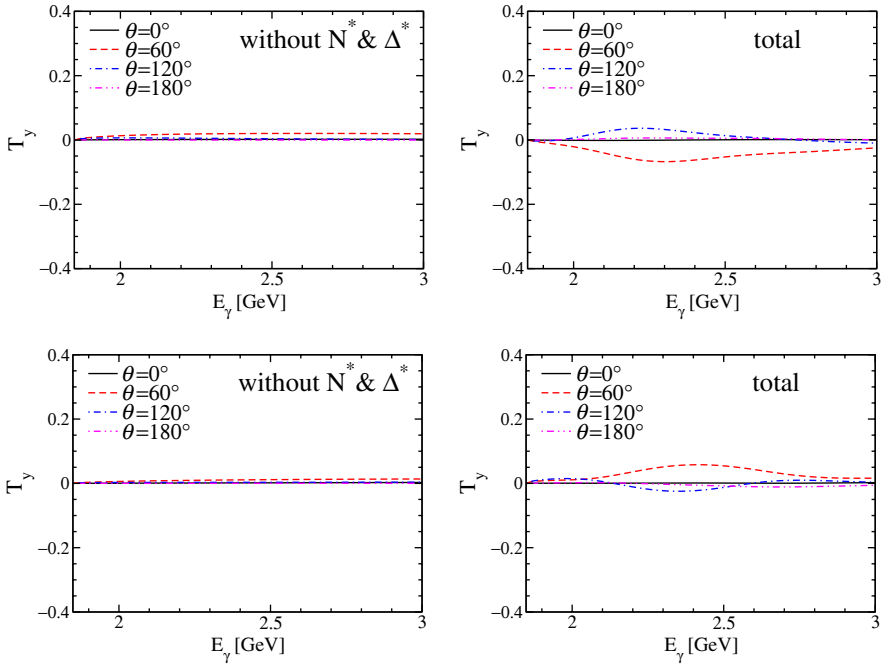

FIG. 11 (color online). In the upper panel, target asymmetries T_y for $\gamma p \to K^{*0}\Sigma^+$ with and without N^* and Δ^* resonances are drawn in order as functions of the photon energy E_γ, the scattering angle being changed from 0° to 180°. In the lower panel, those for $\gamma p \to K^{*+}\Sigma^0$ are shown with and without the resonance contributions, respectively.

IV. SUMMARY AND CONCLUSION

We have investigated $K^*\Sigma(1193)$ photoproduction, employing the effective Lagrangian approach at the tree-level Born approximation. In addition to the Born diagrams, which satisfy the WT identity with the phenomenological form factors, we took into account the baryon-resonance contributions in the s and u channels. All the model parameters were determined by using experimental and theoretical information, reproducing the available experimental data for the present reaction process. We summarize important observations in the present work as follows:

(i) The unpolarized production strengths for $K^{*0}\Sigma^+$ and $K^{*+}\Sigma^0$ photoproductions are negligibly affected by the resonance contributions. In other words, the total production rate is dominated by the Born diagrams such as the Δ-pole and K exchanges, as far as we rely on presently available experimental and theoretical information for the resonances taken into account. This tendency is obviously different from those for $K\Lambda(1116)$ [4] and $K^*\Lambda(1116)$ [19] photoproductions. The total cross section of the $\gamma p \to K^{*+}\Sigma^0$ process turns out to be a little smaller than that of $\gamma p \to K^{*0}\Sigma^+$, because of the isospin factors and the coupling constants.

(ii) The angular dependences of the $K^{*0}\Sigma^+$ channel are qualitatively well reproduced in comparison with the CLAS [14] experiment data, showing that the main dependence comes from the the Δ-pole and K exchanges. On the contrary, that of the $K^{*+}\Sigma^0$ channel is dominated by the Δ-pole contribution in the s channel, showing rather flat curves.

(iii) The single-polarization observables such as recoil and target asymmetries P_y and T_y are mainly described by the N^* and Δ^* resonances, though their effects are almost invisible in the cross sections. The reason lies in the fact that the generic Born and $\Delta(1232)$-exchange contributions play a minor role in the polarized observables. On the contrary, it is difficult to see the resonance contributions in the transversely polarized photon-beam asymmetry Σ_γ, since the electric and magnetic coupling strengths for the γNR, where $R \equiv (N^*, \Delta^*, Y^*)$, are qualitatively similar to each other.

(iv) In the present work, we used the experimental data from the Particle Data Group (PDG) book of 2010. In the latest version of 2012, however, the prediction for the electromagnetic properties of some nucleon resonances, i.e., $D_{13}(2080)$, $S_{11}(2090)$, and $D_{15}(2200)$, have been updated. In the PDG 2012, these resonances are nominated as $D_{13}(1875)$, $S_{11}(1895)$, $D_{15}(2060)$, and $D_{13}(2120)$. We have repeated our calculation by including the latter two resonances, by observing that the effect of the former two is not important because they locate far lower than the threshold. In doing so, we used the new values of the photon helicity amplitude, but the same strong coupling constants as those of $D_{15}(2200)$ and $D_{13}(2080)$. Then, we come to the conclusion that the effects of resonances are within 15% in comparison with the total results.

As noted above, $K^*\Sigma(1193)$ photoproduction manifests obviously different features of the resonance contributions in comparison with other strangeness productions. The present theoretical results (in particular, the single-polarization observables) will provide useful guides for future experiments in understanding the role of higher resonances in photoproductions, which can be measured by the CLAS, LEPS, and CBELSA/TAPS collaborations. The double polarization observables such as the polarization transport coefficients $C_{x,y}$ [41,42] are under progress and appear elsewhere.

ACKNOWLEDGMENTS

The authors are grateful to Y. Oh, K. Hicks, and W. Tang for fruitful discussions and comments for the present work. H. Ch. K expresses his gratitude to R. Woloshyn and P. Navratil for their hospitality during his stay at TRIUMF, where part of the present work was done. The works of S. H. K. and H. Ch. K. were supported by the Basic Science Research Program through the National Research Foundation of Korea funded by the Ministry of Education, Science and Technology (Grant No. 2012001083). S. H. K. is also supported by the Ministry of Education, Culture, Science and Technology of Japan. A. H. is supported in part by the Grant-in-Aid for Scientific Research on Priority Areas titled "Elucidation of New Hadrons with a Variety of Flavors" (Grant No. E01:21105006).

APPENDIX

The scattering amplitude for $K^*\Sigma(1193)$ photoproduction can be written as follows:

$$\mathcal{M} = \varepsilon^*_\nu \bar{u}_\Sigma \mathcal{M}^{\mu\nu} u_N \epsilon_\mu, \tag{A1}$$

where the Dirac spinors of the nucleon and Λ are denoted by u_N and u_Σ, respectively, and ϵ_μ and ε_μ represent the polarization vectors for the photon and the K^*, respectively:

$$\epsilon_\mu = \begin{cases} \epsilon_\parallel = (0,1,0,0) \\ \epsilon_\perp = (0,0,1,0) \end{cases},$$
$$\varepsilon_\mu = \begin{cases} \varepsilon_1 = (0, \cos\theta, 0, -\sin\theta) \\ \varepsilon_2 = (0,0,1,0) \\ \varepsilon_3 = \frac{1}{M_{K^*}}(\boldsymbol{k}_{K^*}, E_{K^*}\sin\theta, 0, E_{K^*}\cos\theta) \end{cases}, \tag{A2}$$

satisfying $\epsilon^2 = \varepsilon^2 = -1$, and otherwise zero.

The relevant invariant amplitudes for each kinematic channel without (N^*, Δ^*) are given as follows:

$$\mathcal{M}_c^{\mu\nu} = -\frac{ie_{K^*}g_{K^*N\Sigma}\kappa_{K^*N\Sigma}}{2M_N}\sigma^{\mu\nu}, \qquad \mathcal{M}_{t(\kappa)}^{\mu\nu} = \frac{-2g_{\gamma K^*\kappa}g_{\kappa N\Sigma}}{t-(M_\kappa - i\Gamma_\kappa/2)^2}(k_1\cdot k_2 g^{\mu\nu} - k_1^\nu k_2^\mu),$$

$$\mathcal{M}_{t(K)}^{\mu\nu} = \frac{ig_{\gamma KK^*}g_{KN\Sigma}}{t-M_K^2}\epsilon^{\mu\nu\alpha\beta}k_{1\alpha}k_{2\beta}\gamma_5,$$

$$\mathcal{M}_{t(K^*)}^{\mu\nu} = \frac{e_{K^*}g_{K^*N\Sigma}}{t-(M_{K^*}-i\Gamma_{K^*}/2)^2}(2k_2^\mu g^{\nu\alpha} - k_2^\alpha g^{\mu\nu} + k_1^\nu g^{\mu\alpha})\left[g_{\alpha\beta} - \frac{(k_1-k_2)_\alpha(k_1-k_2)_\beta}{M_{K^*}^2}\right]\left[\gamma^\beta - \frac{i\kappa_{K^*N\Sigma}}{2M_N}\sigma^{\beta\delta}(k_1-k_2)_\delta\right],$$

$$\mathcal{M}_{s(N)}^{\mu\nu} = \frac{g_{K^*N\Sigma}}{s-M_N^2}\left[\gamma^\nu - \frac{i\kappa_{K^*N\Sigma}}{2M_N}\sigma^{\nu\alpha}k_{2\alpha}\right](\not{k}_1 + \not{p}_1 + M_N)\left[e_N\gamma^\mu + \frac{ie\kappa_N}{2M_N}\sigma^{\mu\beta}k_{1\beta}\right],$$

$$\mathcal{M}_{s(\Delta)}^{\mu\nu} = \frac{f_{K^*\Delta\Sigma}}{s-(M_\Delta - i\Gamma_\Delta/2)^2}\frac{e}{2M_{K^*}}\gamma_\rho\gamma_5(k_2^\beta g^{\nu\rho} - k_2^\rho g^{\nu\beta})\Delta_{\beta\alpha}\left[\frac{g_1}{2M_N}\gamma_\delta - \frac{g_2}{(2M_N)^2}p_{1\delta}\right]\gamma_5(k_1^\alpha g^{\mu\delta} - k_1^\delta g^{\mu\alpha}),$$

$$\mathcal{M}_{u(\Sigma)}^{\mu\nu} = \frac{g_{K^*N\Sigma}}{u-M_\Sigma^2}\left[e_\Sigma\gamma^\mu + \frac{ie\kappa_\Sigma}{2M_N}\sigma^{\mu\alpha}k_{1\alpha}\right](\not{p}_2 - \not{k}_1 + M_\Sigma)\left[\gamma^\nu - \frac{i\kappa_{K^*N\Sigma}}{2M_N}\sigma^{\nu\beta}k_{2\beta}\right]. \tag{A3}$$

Now, we write the corresponding invariant amplitudes for (N^*, Δ^*) for each spin and parity:

$$\mathcal{M}_{s(R)}^{\mu\nu}\left(\frac{1}{2}^\pm\right) = \frac{-ie}{s-M_R^2}\frac{h_{1R_1}}{(2M_N)^2}\left[g_1\frac{M_{K^*}^2}{M_R \mp M_N}\Gamma^{\nu(\mp)} \mp ig_2\Gamma^{(\mp)}\sigma^{\nu\beta}k_{2\beta}\right](\not{k}_1 + \not{p}_1 + M_R)\Gamma^{(\mp)}\sigma^{\mu\alpha}k_{1\alpha},$$

$$\mathcal{M}_{s(R)}^{\mu\nu}\left(\frac{3}{2}^\pm\right) = \frac{e}{s-M_R^2}\left[\frac{g_1}{2M_N}\Gamma_\rho^{(\pm)} + \frac{g_2}{(2M_N)^2}p_{2\rho}\Gamma^{(\pm)} - \frac{g_3}{(2M_N)^2}k_{2\rho}\Gamma^{(\pm)}\right](k_2^\beta g^{\nu\rho} - k_2^\rho g^{\nu\beta})\Delta_{\beta\alpha}(R, k_1+p_1)$$
$$\times\left[\frac{\mu_{R_3}}{2M_N}\Gamma_\delta^{(\pm)} \mp \frac{\bar{\mu}_{R_3}}{(2M_N)^2}\Gamma^{(\pm)}p_{1\delta}\right](k_1^\alpha g^{\mu\delta} - k_1^\delta g^{\alpha\mu}),$$

$$\mathcal{M}_{s(R)}^{\mu\nu}\left(\frac{5}{2}^\pm\right) = \frac{e}{s-M_R^2}\left[\frac{g_1}{(2M_N)^2}\Gamma_\rho^{(\mp)} + \frac{g_2}{(2M_N)^3}p_{2\rho}\Gamma^{(\mp)} - \frac{g_3}{(2M_N)^3}k_{2\rho}\Gamma^{(\mp)}\right]k_2^{\beta_2}(k_2^{\beta_1}g^{\nu\rho} - k_2^\rho\epsilon^{\nu\beta_1})\Delta_{\beta_1\beta_2;\alpha_1\alpha_2}(R, k_1+p_1)$$
$$\times\left[\frac{\mu_{R_5}}{(2M_N)^2}\Gamma_\delta^{(\mp)} \pm \frac{\bar{\mu}_{R_5}}{(2M_N)^3}\Gamma^{(\mp)}p_{1\delta}\right]k_1^{\alpha_2}(k_1^{\alpha_1}g^{\mu\delta} - k_1^\delta g^{\alpha_1\mu}),$$

$$\mathcal{M}_{s(R)}^{\mu\nu}\left(\frac{7}{2}^\pm\right) = \frac{e}{s-M_R^2}\left[\frac{g_1}{(2M_N)^3}\Gamma_\rho^{(\pm)} + \frac{g_2}{(2M_N)^4}p_{2\rho}\Gamma^{(\pm)} - \frac{g_3}{(2M_N)^4}k_{2\rho}\Gamma^{(\pm)}\right]k_2^{\beta_2}k_2^{\beta_3}(k_2^{\beta_1}g^{\nu\rho} - k_2^\rho\epsilon^{\nu\beta_1})$$
$$\times\Delta_{\beta_1\beta_2\beta_3;\alpha_1\alpha_2\alpha_3}(R, k_1+p_1)\left[\frac{\mu_{R_7}}{(2M_N)^3}\Gamma_\delta^{(\pm)} \mp \frac{\bar{\mu}_{R_7}}{(2M_N)^4}\Gamma^{(\pm)}p_{1\delta}\right]k_1^{\alpha_2}k_1^{\alpha_3}(k_1^{\alpha_1}g^{\mu\delta} - k_1^\delta g^{\alpha_1\mu}),$$

$$\mathcal{M}_{u(R)}^{\mu\nu}\left(\frac{3}{2}^+\right) = \frac{f_{K^*N\Sigma^*}^{(1)}}{u-M_{\Sigma^*}^2}\frac{e}{2M_{K^*}}\left[\frac{g_1}{2M_N}\gamma_\rho + \frac{g_2}{(2M_N)^2}p_{2\rho}\right](k_1^\beta g^{\rho\mu} - k_1^\rho g^{\beta\mu})\gamma_5\Delta_{\beta\alpha}\gamma_\delta\gamma_5(k_2^\alpha g^{\nu\delta} - k_2^\delta g^{\alpha\nu}), \tag{A4}$$

where the definitions for $\Gamma^{(\pm)}$ are given in Eq. (14) and each of the decay widths of resonances is included by replacing M_R in the propagator with $M_R - i\Gamma_R/2$. The spin-3/2, 5/2 and 7/2 Rarita-Schwinger spin projections in Eqs. (A3) and (A4) are given by

$$\Delta_{\beta\alpha}(R,p) = (\not{p} + M_R)\left[-g_{\beta\alpha} + \frac{1}{3}\gamma_\beta\gamma_\alpha + \frac{1}{3M_R}(\gamma_\beta p_\alpha - \gamma_\alpha p_\beta) + \frac{2}{3M_R^2}p_\beta p_\alpha\right],$$

$$\Delta_{\beta_1\beta_2;\alpha_1\alpha_2}(R,p) = (\not{p} + M_R)\left[\frac{1}{2}(\bar{g}_{\beta_1\alpha_1}\bar{g}_{\beta_2\alpha_2} + \bar{g}_{\beta_1\alpha_2}\bar{g}_{\beta_2\alpha_1}) - \frac{1}{5}\bar{g}_{\beta_1\beta_2}\bar{g}_{\alpha_1\alpha_2} - \frac{1}{10}(\bar{\gamma}_{\beta_1}\bar{\gamma}_{\alpha_1}\bar{g}_{\beta_2\alpha_2} + \bar{\gamma}_{\beta_1}\bar{\gamma}_{\alpha_2}\bar{g}_{\beta_2\alpha_1}\right.$$
$$\left. + \bar{\gamma}_{\beta_2}\bar{\gamma}_{\alpha_1}\bar{g}_{\beta_1\alpha_2} + \bar{\gamma}_{\beta_2}\bar{\gamma}_{\alpha_2}\bar{g}_{\beta_1\alpha_1})\right],$$

$$\Delta_{\beta_1\beta_2\beta_3;\alpha_1\alpha_2\alpha_3}(R,p) = (\not{p} + M_R)\frac{1}{36}\sum_{P(\alpha),P(\beta)}\left[-\bar{g}_{\beta_1\alpha_1}\bar{g}_{\beta_2\alpha_2}\bar{g}_{\beta_3\alpha_3} + \frac{3}{7}\bar{g}_{\beta_1\alpha_1}\bar{g}_{\beta_2\beta_3}\bar{g}_{\alpha_2\alpha_3} + \frac{3}{7}\bar{\gamma}_{\beta_1}\bar{\gamma}_{\alpha_1}\bar{g}_{\beta_2\alpha_2}\bar{g}_{\beta_3\alpha_3}\right.$$
$$\left. - \frac{3}{35}\bar{\gamma}_{\beta_1}\bar{\gamma}_{\alpha_1}\bar{g}_{\beta_2\beta_3}\bar{g}_{\alpha_2\alpha_3}\right]. \tag{A5}$$

Here, we have used the following notations for convenience:

$$\bar{g}_{\alpha\beta} = g_{\alpha\beta} - \frac{p_\alpha p_\beta}{M^2}, \qquad \bar{\gamma}_\alpha = \gamma_\alpha - \frac{p_\alpha}{M^2}\not{p}. \tag{A6}$$

[1] R. Bradford *et al.* (CLAS Collaboration), Phys. Rev. C **73**, 035202 (2006).
[2] K. Tsukada *et al.*, Phys. Rev. C **78**, 014001 (2008).
[3] T. Watanabe *et al.*, Phys. Lett. B **651**, 269 (2007).
[4] S. Janssen, J. Ryckebusch, D. Debruyne, and T. Van Cauteren, Phys. Rev. C **65**, 015201 (2001).
[5] T. Mart, Phys. Rev. C **83**, 048203 (2011).
[6] B. G. Yu, T. K. Choi, and W. Kim, Phys. Lett. B **701**, 332 (2011).
[7] L. De Cruz, D. G. Ireland, P. Vancraeyveld, and J. Ryckebusch, Phys. Lett. B **694**, 33 (2010).
[8] T. Corthals, J. Ryckebusch, and T. Van Cauteren, Phys. Rev. C **73**, 045207 (2006).
[9] T. Corthals, D. G. Ireland, T. Van Cauteren, and J. Ryckebusch, Phys. Rev. C **75**, 045204 (2007).
[10] L. Guo and D. P. Weygand (CLAS Collaboration), arXiv: hep-ex/0601010.
[11] K. Hicks, D. Keller, and W. Tang, AIP Conf. Proc. **1374**, 177 (2011).
[12] M. Nanova *et al.* (CBELSA/TAPS Collaboration), Eur. Phys. J. A **35**, 333 (2008).
[13] I. Hleiqawi and K. Hicks, arXiv:nucl-ex/0512039.
[14] I. Hleiqawi *et al.* (CLAS Collaboration), Phys. Rev. C **75**, 042201 (2007); **76**, 039905(E) (2007).
[15] S. H. Hwang *et al.* (LEPS Collaboration), Phys. Rev. Lett. **108**, 092001 (2012).
[16] Y. Oh and H. Kim, Phys. Rev. C **73**, 065202 (2006).
[17] Y. Oh and H. Kim, Phys. Rev. C **74**, 015208 (2006).
[18] S. Ozaki, H. Nagahiro, and A. Hosaka, Phys. Rev. C **81**, 035206 (2010).
[19] S. H. Kim, S. i. Nam, Y. Oh, and H.-Ch. Kim, Phys. Rev. D **84**, 114023 (2011).
[20] Q. Zhao, J. S. Al-Khalili, and C. Bennhold, Phys. Rev. C **64**, 052201 (2001).
[21] K. Nakamura (Particle Data Group), J. Phys. G **37**, 075021 (2010).
[22] Y. Oh, C. M. Ko, and K. Nakayama, Phys. Rev. C **77**, 045204 (2008).
[23] V. G. J. Stoks and T. A. Rijken, Phys. Rev. C **59**, 3009 (1999).
[24] S. Capstick, Phys. Rev. D **46**, 2864 (1992).
[25] S. Capstick and W. Roberts, Phys. Rev. D **58**, 074011 (1998).
[26] H. Haberzettl, C. Bennhold, T. Mart, and T. Feuster, Phys. Rev. C **58**, R40 (1998).
[27] R. M. Davidson and R. Workman, Phys. Rev. C **63**, 025210 (2001).
[28] H. Haberzettl, K. Nakayama, and S. Krewald, Phys. Rev. C **74**, 045202 (2006).
[29] D. Black, M. Harada, and J. Schechter, Phys. Rev. Lett. **88**, 181603 (2002).
[30] W. Rarita and J. Schwinger, Phys. Rev. **60**, 61 (1941).
[31] B. J. Read, Nucl. Phys. **B52**, 565 (1973).
[32] R. Machleidt, K. Holinde, and C. Elster, Phys. Rep. **149**, 1 (1987).
[33] V. V. Molchanov *et al.* (SELEX Collaboration), Phys. Lett. B **590**, 161 (2004).
[34] R. H. Hackman, N. G. Deshpande, D. A. Dicus, and V. L. Teplitz, Phys. Rev. D **18**, 2537 (1978).
[35] J. W. Darewych, M. Horbatsch, and R. Koniuk, Phys. Rev. D **28**, 1125 (1983).
[36] C. L. Schat, C. Gobbi, and N. N. Scoccola, Phys. Lett. B **356**, 1 (1995).
[37] A. Abada, H. Weigel, and H. Reinhardt, Phys. Lett. B **366**, 26 (1996).
[38] G. Wagner, A. J. Buchmann, and A. Faessler, Phys. Rev. C **58**, 1745 (1998).
[39] H.-Ch. Kim, M. Polyakov, M. Praszalowicz, G.-S. Yang, and K. Goeke, Phys. Rev. D **71**, 094023 (2005).
[40] A. I. Titov and T. S. H. Lee, Phys. Rev. C **66**, 015204 (2002).
[41] R. Bradford *et al.* (CLAS Collaboration), Phys. Rev. C **75**, 035205 (2007).
[42] S. i. Nam, Phys. Rev. C **81**, 015201 (2010).